

Deep Semantic Instance Segmentation of Tree-like Structures Using Synthetic Data

Kerry Halupka

IBM Research, Level 22/60 City Rd, Southbank, Victoria, Australia.

kerry.halupka@a1.ibm.com

Rahil Garnavi

IBM Research, Level 22/60 City Rd, Southbank, Victoria, Australia.

rahilgar@a1.ibm.com

Stephen Moore

IBM Research, Level 22/60 City Rd, Southbank, Victoria, Australia.

stevemoore@a1.ibm.com

Abstract

Tree-like structures, such as blood vessels, often express complexity at very fine scales, requiring high-resolution grids to adequately describe their shape. Such sparse morphology can alternately be represented by locations of centreline points, but learning from this type of data with deep learning is challenging due to it being unordered, and permutation invariant. In this work, we propose a deep neural network that directly consumes unordered points along the centreline of a branching structure, to identify the topology of the represented structure in a single-shot. Key to our approach is the use of a novel multi-task loss function, enabling instance segmentation of arbitrarily complex branching structures. We train the network solely using synthetically generated data, utilizing domain randomization to facilitate the transfer to real 2D and 3D data. Results show that our network can reliably extract meaningful information about branch locations, bifurcations and end-points, and sets a new benchmark for semantic instance segmentation in branching structures.

1. Introduction

In this work, we are interested in the problem of extracting topological information from thin, branching structures, such as blood vessels, neurons, and trees in nature. The complexity of these structures is often expressed at a very fine scale, meaning that a high resolution, sparsely filled grid would be required to adequately describe their shape with pixels or voxels, making analysis computationally ex-

pensive. A possible solution to this issue is to represent the structures as centreline points in Euclidean Space, which would convert the large, sparse grid to a manageable form that allows more fine-grained structure to be represented. However, dealing with a set of points that are unordered and permutation invariant introduces some challenges. In particular, traditional deep learning architectures for geometric 3D data normally operate by exploiting relationships between neighbouring voxels, which are not present in point cloud data.

The possibility of using deep networks to reason about points has been explored, resulting in networks that process point sets for the purpose of class labelling, part or semantic segmentation [16, 17]. However, these networks either do not consider local information at all, instead relying on global pooling to embed relationships between individual points and the overall structure [16], or they extract local and global features by progressively growing scales in a hierarchical fashion [17]. The latter approach has proved to be effective for processing solid, predominantly convex shapes, such as animals and furniture, but is not optimal for thin, complex structures. This is because reasoning over local neighbourhoods of points may inadvertently include nearby, disconnected branches but not current branch end points. Additionally, we aim to extract meaningful topological information such as the location of junction points, the number of individual branches, and the branches to which each point belongs, which requires a loss function that is invariant to the number of branches.

To meet these challenges, we present a data-driven topology estimation deep neural network that operates on unordered 2D or 3D centreline coordinates of thin, tubular,

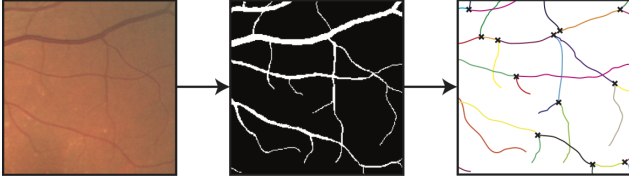


Figure 1. Workflow of instance segmentation of blood vessels in a retinal fundus image. After segmentation, centreline coordinates of vessels are extracted using skeletonisation, and input in random order to the proposed network. Right-most image shows the output of the network with point colour indicating branch membership, and identified branch end points indicated by crosses. (Best viewed in colour)

branching structures (Figure 1). We train our network using a novel multi-task learning framework to jointly develop branch and end-point identification abilities. Branches and end-points are identified using standard point-wise softmax loss, while individual branch instances are separated with a discriminative loss function [4] operating at the point level. The latter allows the network to cluster an arbitrary number of branches, which can be identified in a post-processing step. The proposed network architecture, named Branch-Net, is applied to the entire structure at once, helping it to develop a global reasoning and context for branch membership, but has local feature aggregation to inform junction localisation. Due to the intensive nature of the annotations required to train and validate the method, we train the network solely with synthetic data. However, we show that by applying domain randomization [25, 26] in the data generation step, the performance translates well to real blood vessel structures. The key contributions of our work are as follows:

- We propose a simple but effective means of embedding global structural information in point-based neural networks.
- We introduce a novel framework which enables the application of instance segmentation, the task of simultaneously solving object detection and semantic segmentation, to unordered point-cloud data. To the best of our knowledge, there are no prior works focusing on this problem.
- We employ extensive domain randomization during point-cloud generation to successfully transfer the networks success on to real data, without domain adaptation, fine-tuning, or having been exposed to real data during training.
- We provide a thorough sensitivity analysis showing that our proposed method is robust to multiple types of noise, with equal performance on 2D and 3D structures.
- We conduct an ablation study to investigate the importance of each domain randomisation parameter on the transfer to real data.

2. Related Work

2.1. Unstructured Point Clouds

Point sets are unordered and not structured in a grid, therefore do not inherently favour a deep learning-based approach to processing. Therefore, for analysis with CNN’s, previous works have transformed point clouds into uniform grids through rasterization [29, 28], or represented them in kd-tree format [9]. More recent work has made progress towards directly consuming point-sets within a deep-learning framework. A pioneer in the field was PointNet, which returned a whole-set class label, or point-wise segmentation labels for a given point set [16]. However, the particularly inspiring work was PointNet++, which introduced a hierarchical feature learning architecture to mimic the progressively growing receptive fields of convolutional neural networks, enabling the network to capture local geometry context. We further improve this network structure by including global feature descriptors along with local, and defining a novel multi-task loss function to enable instance segmentation.

2.2. Instance Segmentation

A key difficulty associated with the naive application of a softmax cross-entropy loss function to branch instance identification is the requirement for a constant number of branches (and therefore classes), with a specific hierarchical structure, which may not hold true for particular structures, such as trees in nature. This could be addressed by imposing an upper limit to the number of branches that can be detected, however this would limit the representational power of the network, and introduce imbalances in class representation. Therefore, we propose the use of a discriminative loss function to enable semantic instance segmentation of points into branches. Our loss function is inspired by [4], where pixels in a masked image were mapped to a location in feature space close to other pixels composing the same object, but away from those representing others. Separate instances are then identified with a post-processing operation. Other forms of instance segmentation have also been proposed, including pipelines with region or object proposals followed by segmentation [3, 18], and end-to-end recurrent neural networks that perform object detection and segmentation [21, 12, 18]. In contrast to these works, our method treats the input structure holistically, which is required in case of crossing branches, and is conceptually simpler and easier to implement than recurrent networks.

2.3. Extraction of Topological Information

Several methods exist for extracting meaningful topological information from thin, tree-like structures, however no generic frameworks perform equally on both 2D and 3D structures. Successful approaches for 2D data tend to in-

clude multi-stage pipelines where regions of interest are identified and then classified. These include [10] and [1], where directional filters to identify regions of interest are followed by optimisation to classify, and [15], where a convolutional neural network is used to identify patches of interest, followed by a further neural network to classify said patches. By taking as input larger section of structures our network is able to develop a global reasoning and context for bifurcation locations and branches.

Previous approaches applied to 3D data have involved combined segmentation and topology estimation by growing an area outwards from a seed point, guided by image-derived constraints [2, 6, 22]. This approach can experience early termination in the presence of intensity inhomogeneity, and noisy images. In contrast, our algorithm does not operate on seed points, and is therefore not negatively influenced by suboptimal seed point placement. Additionally, since our network is not informed by image-based features, it is not impacted by circumstances where local image features indicate a discontinuity, or the radius experiences local changes. Since our model operates on only a skeletonised branched structure, it is task-independent, and could in theory be applied as a post-processing step following segmentation and skeletisation, in any domain involving branching structures. Furthermore, our network is a generic framework that can operate on both 2D and 3D structures.

2.4. Training on Synthetic Data

Use of synthetic data to train neural networks is an attractive proposition, particularly for work requiring complex annotations, where large, fully-annotated datasets are not available. Previous image-based work has attempted to make the generated data match the real data as closely as possible, by using high quality renderers [7]. However, this often still fails to accurately match the statistics of real data. Several approaches have emerged to tackle the problem of domain adaptation, including re-training in the target domain [30], learning invariant features between domains [27], and learning a mapping between domains [23]. Alternatively, domain randomization has been proposed [25], where synthetic data is generated with sufficient variation at training time that the network is able to generalize to real-world data at test time. This process removes the need for domain adaptation, and has been used successfully for object detection and classification [13, 25, 26], and training robotic control processes [24, 14]. This approach is particularly well suited to our application, since large, well-annotated datasets are not available, and randomization can be easily introduced in to the generation process of branching structures through structural changes, point jittering and dropout.

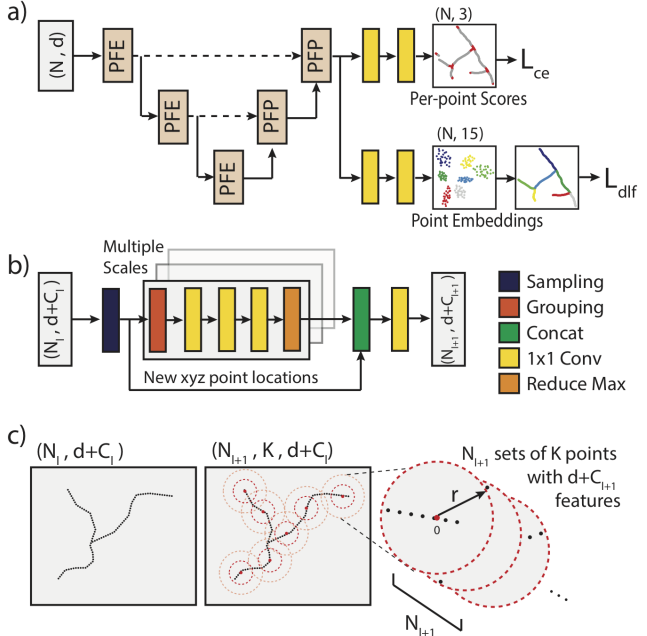


Figure 2. Illustration of the proposed BranchNet architecture using a 2D tree-like structure as an example. a) The overall hierarchical architecture with task specific shared fully connected layers and objectives. Dashed lines indicate skip connections. b) Expanded view of the Point Feature Embedding (PFE) layer. c) Graphical representation of sampling procedure. (Best viewed in colour)

3. Proposed Method

Suppose a thin, branching structure is represented by an unordered set of 3D points $\{P_i | i = 1, 2, \dots, N\}$, where each point P_i is a vector of its (x, y, z) 3D location along the centreline of the structure. We are interested in the topology of the structure represented by these points, including which points belong to each branch, and the location of branch end points, in the form of semantic labels. Towards this end, we propose BranchNet, a deep neural network that directly consumes unordered points along the centreline of a branching structure, to identify the topology of the represented structure in a single-shot.

3.1. Network Architecture

The structure of the network is shown in Figure 2a. Our network is composed of two main components: *Point Feature Embedding (PFE)* and *Point Feature Propagation (PFP)*, which can be considered as an encoder and a decoder, respectively, and are further explained in the following.

3.1.1 Point Feature Embedding

The PFE component (Figure 2b) maps the raw 3D coordinates to a feature space by hierarchically aggregating information at multiple scales. It is inspired by the set abstrac-

tion process described in [17], but includes global feature descriptors along with local. The input to a PFE component l is a matrix of size $N_l \times (d + C_l)$, where N_l is the number of points with d -dim coordinate and C_l -dim point features. It outputs a $N_{l+1} \times (d + C_{l+1})$ matrix of N_{l+1} subsampled points, selected using farthest point sampling from the original set, with C_{l+1} new point features summarising local and global context (Figure 2c). The local neighbourhood around each point N_{l+1} is encoded by translating the K points in a radius of r around each point into a frame relative to the centroid point. The feature vector of each point is updated with three shared fully connected (FC) layers, similar to 1×1 convolutions, followed by max pooling over the K points. We use Multi-Scale Grouping proposed in [17] to acquire point features at multiple scales. However, in contrast to [17], we then concatenate the local features at each of the scales with the Cartesian coordinates of each sampled point, followed by a further shared FC layer. These locations are used as global point features, and serve to inform the network of relative point positions. Additionally, this small skip-connection aids in the training by improving gradient flow.

3.1.2 Point Feature Propagation

To obtain features for all the original points, we propagate features from the subsampled points to the original points, as described in [17]. Briefly, point features are interpolated from N_l points to N_{l-1} points, and then concatenated with the skip-link point features, see [17] for more details. The features for each point are then updated using two (for the first two PFP layers) or three (for the final PFP layer) shared FC layers.

3.1.3 Task-dependent Layers

Feature propagation back to the original points is followed by several task-specific layers, without shared weights, as shown by yellow blocks in Figure 2a). BranchNet is tasked with grouping points based on which branch they lie within a structure, as well as which points are close to branch end points. These tasks are separate but complimentary. Intuitively, the most difficult points to group are those near junctions (where multiple branches meet). Tasking part of the network with specifically locating these points forces attenuation, resulting in better branch cluster separation.

3.2. Multi-Task Learning

The BranchNet loss function comprises two parts: loss of point-wise semantic segmentation of branch end points from branches (L_{ce}), and the loss associated with instance segmentation of branches (L_{dlf}),

$$L = L_{ce} + wL_{dlf}, \quad (1)$$

where w is a weighting parameter to control the trade-off between the two components of the loss. During training, we pad our point sets such that the training set has a consistent number of points (10,000). Therefore, our dataset contains three classes of points: padding, branch and end-point. L_{ce} is calculated using point-wise cross-entropy on the soft-max output of the upper branch in Figure 2a).

We use a discriminative loss function [4] to calculate the instance segmentation loss L_{dlf} (Eq. 2). This method allows for single-shot instance detection with feed-forward networks, avoiding the inefficiencies of detect-and-segment approaches. This loss function encourages points with the same label (therefore the same instance) to be projected to nearby locations in feature space, while embedding's with different labels would be represented far apart. This is achieved by applying two competing forces on an embedding: a variance force (L_{var} , Eq. 3) that pulls points towards their cluster mean, and distance force (L_{dist} , Eq. 4) pushing different clusters apart. Here, C is the number of clusters, μ_c is the mean of cluster c which has N_c elements, and x_i is an embedding. These forces are hinged (denoted by $[x]_+ = \max(0, x)$) such that embedding's within a distance of δ_v from their cluster centre are not pulled towards it, and those further than δ_d away are not repulsed. The overall loss, also contains a regularising term that pulls all clusters towards the centre.

$$L_{dlf} = \alpha \cdot L_{var} + \beta \cdot L_{dist} + \gamma \cdot \frac{1}{C} \sum_{c=1}^C \|\mu_c\|, \quad (2)$$

$$L_{var} = \frac{1}{C} \sum_{c=1}^C \frac{1}{N_c} \sum_{i=1}^{N_c} [\|\mu_c - x_i\| - \delta_v]_+^2, \quad (3)$$

$$L_{dist} = \frac{1}{C(C-1)} \sum_{c_A=1}^C \sum_{c_B=1}^C [2\delta_d - \|\mu_c - x_i\|]_+^2 \quad \forall c_A \neq c_B. \quad (4)$$

This formulation results in all point embedding's being located within δ_v from the centre of their associated cluster, and at least $2\delta_d$ from the centres of all other clusters, provided the loss has converged. At test time this assumption may not be accurate, so we apply a fast variant of the mean-shift algorithm [5] to locate and threshold around cluster centres.

We train the network with margins of $\delta_v = 0.7$, and $\delta_d = 1.5$, and 15 output dimensions. The weight parameters were set to $w = 0.05$ (for Eq. 1), $\alpha = 1.5$, $\beta = 1$ and $\gamma = 0.001$ (for Eq. 4). The Adam training algorithm [8] was used for end-to-end training with mini-batch size of 12 and learning rate of $1e-5$.

We use PFE, PFP and TD to represent point feature embedding, point feature propagation, and task dependent

layers, respectively. Parameters for each of the layers in BranchNet are shown in Table 1, with m scales, K local regions of ball radius r . $[l_1, \dots, l_d]$ represents the d FC layers with width l_i ($i = 1, \dots, d$), and g is the width of the FC layer following concatenation of local point features with global location. Both TD branches acquire features from the final PFP layer, and $R = 4e - 3$. All FC layers are followed by batch normalization and ReLU except for the last layer in each TD path.

Table 1. BranchNet parameters

#	Layer Type	K	m	r	l^1, \dots, l^d	g
1	PFE	512	1	1R	32, 32, 64	128
			2	4R	64, 64, 128	
			3	16R	64, 96, 128	
2	PFE	128	1	4R	64, 64, 128	256
			2	16R	128, 128, 256	
			3	64R	128, 128, 256	
3	PFE	1	-	-	256, 512, 1024	-
4	PFP	-	-	-	256, 128	-
5	PFP	-	-	-	128, 128, 128	-
6	TD1	-	-	-	128, 15	-
7	TD2	-	-	-	128, 3	-

4. Experiments

We train our model on synthetically generated, branching tree structures (Figures 3 and 4). Both 2D and 3D structures are used to train separate networks, which are evaluated using real data.

4.1. Synthetic Data

Synthetic data provides the opportunity to train our approach on highly complex structures similar to those existing in nature, such as neurons and blood vessels, but without undergoing the extensive manual annotations required herein. Domain randomization during data generation results in a large range of inputs, compared to which real data is considered just another variation. Training data was generated by a recursive branching process, with random step lengths and angles to simulate structures with varying degrees of tortuosity. Each structure begins with the same seed point ($x = (0, 0, 0)$) and growth direction ($\theta = 0$, $\phi = 0$ using spherical coordinates). Trees were then grown by randomly varying the following aspects of morphology:

- Number of branching levels (up to 4 levels, chosen with equal probability)
- Bifurcation or trifurcation (80% versus 20% of junctions respectively)
- Start angle of each branch (uniform probability from $[0^\circ, 90^\circ]$)

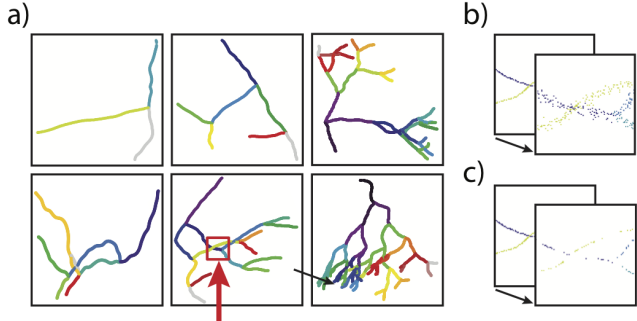


Figure 3. Examples of branching structures used as inputs to the network. Points are coloured according to their branch membership. b,c) Zoomed in versions of the region indicated by the arrow, with varying amounts of point jitter (b, jitter standard deviations shown here are 0-4 pixels) and point dropout (c, 0-75% dropout shown). (Best viewed in colour)

- Number of steps in each branch (Gaussian distribution, mean of 20, standard deviation of 8)
- Angle of each step (Gaussian distribution with mean equal to the angle of the previous step and standard deviation drawn with uniform probability from $[10^\circ, 60^\circ]$)
- Length of each step (uniform probability from $(0, 1]$)

Randomisation of both the number of steps in a branch and the length of each step produces branches with varying degrees of tortuosity. A spline is then fitted through the points, with clamped end points and angles. Example structures are shown in Figure 3a. For 2D data, only ϕ is changed each step with $\theta = 0$. The generated structures were randomly rotated and scaled to lie within a $512 \times 512 \times 512$ cube (or square for 2D data), and rounded to the nearest integer (to approximate voxels or pixels). Duplicate points, such as those occurring at cross-over points, were removed, and the remaining points jittered. For training, we applied point jittering by randomly sampling point offsets from a Gaussian with standard deviation of 3 pixels, and point dropout with a probability of 0.4. The effect of varying levels of point jitter and dropout (examples shown in Figures 3b and c) were tested during evaluation on 1000 unseen randomly generated structures. Point sets were then scaled to unit width, and point order randomised. This produces an infinite data source of thin tree-like structures that are unorganized and scattered, with unknown connectivity.

4.2. Real Data

We tested the trained 2D and 3D networks on two separate, publicly available datasets. The 2D network was evaluated on retinal vasculature segmented from fundus images in the DRIVE dataset [20]. For 5 images within the test dataset, branches and branch end points were annotated manually by a human observer and checked for accuracy by a trained expert. Rather than using ground truth segmen-

tations as input, we use the output of a pre-trained U-net¹ so as to encompass any inaccuracies arising from segmentation (such as disconnected branches), thereby mimicking the use of BranchNet in a real use case. The centreline was then obtained using skeletonisation. This process is shown visually in Figure 1. 36 overlapping patches were taken from each of the images to limit the number vessels shown within each patch, and to increase the size of the test set. The 3D network was evaluated on a centreline model of left and right coronary trees from a segmentation of a computed tomography scan (CTCA) [11]. The left and right trees are treated as separate point sets, resulting in a dataset size for testing of 2. Patches were not obtained to extend the dataset (as per the 2D data), due to the limited number of branches available in each set. Therefore, to artificially enhance the size of this dataset, the prediction for each structure was repeated 50 times, with randomised rotations of the structure. Point sets for both datasets were then scaled to unit width, and point order randomised.

4.3. Evaluation Metrics

To evaluate the success of instance segmentation we report two metrics defined in [19]: Symmetric Best Dice (SBD) and Absolute Difference in Count (DiC). Symmetric Best Dice is computed by first finding, for each input label, the ground truth label yielding the maximum Dice score. These scores are then averaged over input labels, and termed the “Best Dice” score. The “symmetric” element is introduced by repeating the process for each ground truth label paired with its most favourable input label, the minimum Best Dice score between the measures is the SBD. The Absolute Difference in Count is the absolute mean of the difference between the predicted number of branches and the ground truth over all images (lower is better). In a test situation, the location of each individual bifurcation may be required, which is not immediately accessible if multiple points describe each bifurcation. Therefore, we identify clusters of points labelled at bifurcations by performing mean-shift clustering on these points. Ideally, cluster centres will align with actual bifurcation locations. To quantify the success of bifurcation localisation we define the Cluster-based Dice Score (DS_C):

$$DS_C = \frac{2 TP_C}{2 TP_C + FP_C + FN_C}, \quad (5)$$

where TP_C , FP_C and FN_C respectively indicate the number of ground truth clusters correctly predicted, clusters predicted incorrectly, and ground truth clusters missed in the prediction.

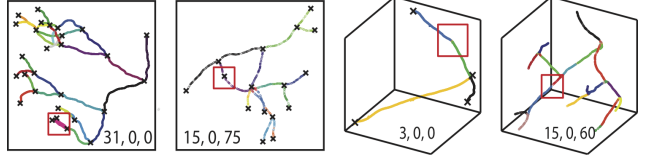


Figure 4. Examples of BranchNet outputs. Points are coloured according to their predicted branch membership, crosses indicate predicted bifurcation and end point locations. Numbers shown in each image indicate: Number of branches, jitter standard deviation (in pixels), point dropout percentage. Red boxes highlight mistakes of interest. (Best viewed in colour)

5. Results and Discussion

5.1. Comparison of Architectures

In this section we compare the performance of the proposed BranchNet (BNet) to those of PointNet++ with Multiscale Grouping (PN++) [17], appended with the proposed task-dependent layers and multi-task loss function. PointNet Vanilla [16] and PointNet++ with Multiresolution Grouping [17] were also tested, but showed reduced performance for all tasks, and are therefore not shown here for brevity.

5.1.1 Synthetic Data

We investigate the impact of varying structural complexities, noise and sampling density, by increasing the numbers of branches in the synthetically generated structures, and amounts of point jitter and point dropout, respectively. Example results for our method applied to synthetic data during test time are shown in Figure 4.

To investigate the robustness of the network to structural complexity, we tested it against 1000 structures at each of 4 different levels of branching (bifurcations only), but no jittering or dropout. Results are shown in Table 2. Interestingly, SBD results show that instance segmentation was more accurate for mid-range complexity structures. This is likely due to the longer branch length of simpler structures, resulting from structure normalisation prior to the network input. This may cause the entire branch to not be covered by the lowest resolution of grouping, and be falsely considered as multiple branches, as shown in Figure 4. However, bifurcations are clearly more difficult to accurately identify with higher numbers of branches, as is evidenced by the lower DS_C results for higher complexity levels. This is unsurprising, given that the likelihood of crossover points (which are a confounding factor) increases with branch numbers. The results also show that for all complexity levels our network outperforms PointNet++.

We randomly drop increasing numbers of points during test time to validate our network’s robustness to non-uniform and sparse data (results shown in Table 3). For this section and the next, we tested against 1000 structures (at

¹<https://github.com/orobix/retina-unet>

Table 2. Structural Complexity Results

		2D		3D	
# Branches		PN++	BNet	PN++	BNet
SBD	3	52.4	55.2	30.0	48.0
	7	52.5	57.5	42.0	71.1
	15	54.5	67.7	46.6	61.3
	31	54.2	67.5	45.1	50.1
DiC	3	3.2	1.2	11.0	1.4
	7	7.5	2.9	13.4	3.2
	15	9.6	3.4	15.7	4.4
	31	10.0	7.6	14.5	12.1
DS _C	3	78.0	84.1	98.7	99.0
	7	97.3	99.8	98.6	98.9
	15	95.6	98.9	98.3	98.8
	31	89.8	94.6	97.0	97.9

Table 3. Sampling Density Results, #Branches = 15

		2D		3D	
Dropout (%)		PN++	BNet	PN++	BNet
SBD	30	67.8	67.6	41.3	63.0
	45	67.5	67.5	40.8	62.7
	60	66.3	68.1	39.7	61.2
	75	62.5	67.8	37.1	56.1
DiC	30	4.0	2.9	4.3	2.7
	45	4.3	3.0	6.7	2.9
	60	4.4	2.9	8.1	2.6
	75	5.1	3.4	11.2	3.2
DS _C	30	98.7	99.0	98.6	98.9
	45	98.6	98.9	98.3	98.8
	60	98.3	98.8	97.0	97.9
	75	97.0	97.9	86.5	87.6

Table 4. Sampling Noise Results, #Branches = 15

		2D		3D	
St. Dev (px)		PN++	BNet	PN++	BNet
SBD	1	50.6	67.2	35.4	62.5
	2	49.7	68.4	34.1	61.7
	3	46.9	72.5	32.7	64.6
	4	41.5	78.6	30.0	65.5
DiC	1	7.0	3.7	5.9	4.7
	2	13.9	3.4	11.1	5.5
	3	16.8	2.9	20.4	6.8
	4	22.3	7.2	29.0	13.7
DS _C	1	94.6	99.2	76.6	78.0
	2	94.2	99.4	97.3	97.3
	3	90.5	98.7	95.1	95.7
	4	77.8	92.7	68.4	89.8

each perturbation level) with the 3rd level of branching (bifurcations only, 15 branches in total). Our network outperformed PointNet++, however the results were considerably closer. This is unsurprising since both models select point

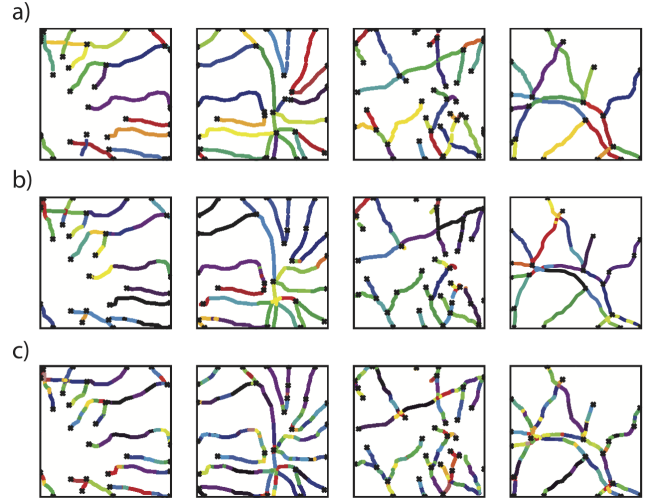


Figure 5. Examples from processing of real 2D retinal vasculature data. Displayed are the ground truth (a), the output of BranchNet (b) and the output of PointNet++ (c).

neighbourhoods at multiple scales, and learn how to weight them. This means that even if nearby points are missing, the available points can agglomerate features with more distant points. These results are particularly impressive given that this level of point dropout would most likely severely disrupt any traditional means of branch tracing.

To evaluate our network’s sensitivity to noisy data we jitter the point locations by sampling from zero-centred Gaussians with increasing standard deviations (results shown in Table 4). Jittering reduces the information inherent in local point features, which has a particularly negative effect on thin, tortuous structures. By including global information in BranchNet, we allow the network to reason over nearby groups of points. This is borne out by the improved bifurcation localisation results for our method. Additionally, including global information ensures that branches with similar structural features (such as angle and tortuosity) are less likely to be mistakenly clustered together. This is shown by the improved performance in the instance segmentation task. However, there remains room for improvement, especially when considering the poor DiC results for 3D structures with large amounts of jitter, likely due to the model predicting that connected branches were split.

5.1.2 Real Data

To evaluate the accuracy of our learned topology estimator in the real world, we use two datasets comprising branching networks of blood vessels. For the network trained for 2D data, we use patches of retinal vasculature obtained through segmentation of fundus images. Examples of the output of BranchNet and PointNet++ on this test set are shown in Figure 5b and c, respectively (ground truth shown in Figure 5a). Summary metrics are shown in Table 5.

Table 5. Aggregated results on real data for PointNet++ (PN++) and BranchNet (BNet).

	2D		3D	
	PN++	BNet	PN++	BNet
SBD	34.6	59.3	44.4	63.7
DiC	38.6	4.14	6.09	4.23
DSC	85.6	94.3	82.2	95.5

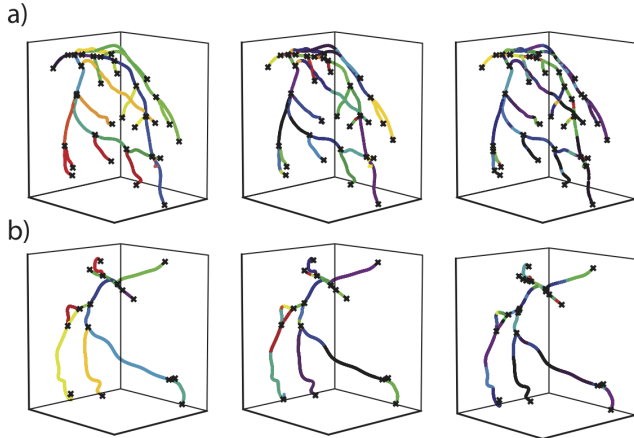


Figure 6. Examples from processing of real 3D coronary artery data. Displayed are the ground truth (column 1), the output of BranchNet (column 2) and the output of PointNet++ (column 3), for both structures in the dataset (a and b).

The results show that even though our model has never been exposed to real data, it is able to successfully identify individual branches and their end points, which is reflected in the SBD, DiC and DSC scores, which are on par with those for synthetic data. Furthermore, the results show that the model can distinguish between crossover points and bifurcations, and tends not to classify points near cross-overs as junctions. Impressively, the model is able to generalize to branches that are disconnected from the main structure (given that such branches were not included in the training set). Additionally, BranchNet visually outperforms PointNet++ (Figure 5c) on the basis of instance segmentation, as shown by the increased number of incorrectly identified branches in PointNet++. However, both networks produced comparable results for identification of junction points, though BranchNet produced less false positives.

Examples of the performance of BranchNet on real 3D data are shown in Figure 6. The network successfully identified all branch end points. However, sometimes it also classified points mid-way along branches incorrectly, resulting in bifurcation false negatives, and lowering the Cluster-based Dice Score. This was more common for PointNet++.

The most common failure of the model is splitting a single branch in to multiple instances. This failure was also apparent on synthetic data, and may be due to the lowest resolution of point grouping in the network not covering the entire branch. This particular failure points to an inherent

limitation of single shot neural networks in this application. Future work will investigate methods of solving this by imbuing the network with more power to reason over different scales, such as the multi-branch convolutional network used by [31] for the purpose of super-resolution. Additionally, future studies will investigate the use of including other features in to the point representation to strengthen relationships between points on the same branch. For example, including further dimensions for radius (at each point along the centreline) and image-based features such as RGB values of the respective pixels.

5.2. Ablation Study

To study the effects of individual domain randomization parameters, we performed an ablation study by systematically omitting them one at a time. We used the same parameters as in the previous sections, but trained four additional versions of BranchNet for each 2D and 3D structures, each time fixing one of the following parameters in the synthetic data: branch length, number of branches (bifurcations only, 15 branches in total), point jitter (set to zero), or point dropout (set to zero). Table 6 shows the results of omitting each of these individual components. We found that the method is sensitive to all of the factors, however the importance of each factor is dependent on dimensionality of the data. The success on 2D data was most dependent on randomisation of the number of branches, which reflects the large variability in number of visible branches in real data.

The 3D data accuracy was most negatively affected by fixing branch length in the synthetic training data. This reflects the large range in branch length of the structures. The 3D network displayed the best performance on SBD when number of branches was fixed, despite the test structures having more branches than the fixed number (15). Given the small size of the evaluation dataset for 3D data, we can not be confident in the generalizability of our ablation test results. In the future, it would be preferable to perform the analysis using a larger dataset. Overall, relevant domain randomization parameters were clearly highly dependent on the particular dataset, but in most cases full randomization was most successful. However, performance was reduced compared to synthetic data. This suggests that the training structures do not fully encompass the range of real data, even with domain randomization. In future studies we will investigate further randomization parameters, and the inclusion of other types of thin, tortuous network structures, not limited to those branching from a single seed point.

6. Conclusion

In this work, we proposed a novel deep learning based approach to automatically extract topological information from unsorted point clouds of thin tree-like 2D and 3D structures. To analyse structures with arbitrary numbers

Table 6. Real 2D and 3D data test results for BranchNet trained on synthetic data with individual domain randomization parameters omitted. Normal refers to full parameter randomization.

Fixed Param.	2D			3D		
	SBD	DiC	DS _C	SBD	DiC	DS _C
normal	59.3	4.14	94.3	63.7	4.23	95.5
length	54.2	5.42	91.5	59.5	7.21	86.4
jittering	54.1	8.13	93.6	62.1	4.48	94.7
# branches	49.4	15.4	87.1	65.8	5.09	93.2
dropout	54.2	5.75	88.2	61.0	6.77	88.1

of branches we proposed a novel, multi-task loss function, incorporating cross-entropy and discriminative losses. We trained the network using extensive domain randomization applied to synthetically generated tree-like structures, and showed that it successfully transferred to real data. In the future, it would be interesting to apply this network to higher dimensional spaces where CNN architectures would be computationally unfeasible, such as time-varying 3D structures.

References

- [1] S. Abbasi-Sureshjani, I. Smit-Ockeloen, E. Bekkers, B. Dashtbozorg, and B. t. H. Romeny. Automatic detection of vascular bifurcations and crossings in retinal images using orientation scores. In *Proceedings of the IEEE 13th International Symposium on Biomedical Imaging (ISBI)*, pages 189–192. IEEE, apr 2016.
- [2] A. Choromanska, S.-F. Chang, and R. Yuste. Automatic reconstruction of neural morphologies with multi-scale tracking. *Frontiers in Neural Circuits*, 6:25, jun 2012.
- [3] J. Dai, K. He, and J. Sun. Instance-aware semantic segmentation via multi-task network cascades. In *Proceedings of the IEEE Conference on Computer Vision and Pattern Recognition*, pages 3150–3158, 2016.
- [4] B. De Brabandere, D. Neven, and L. Van Gool. Semantic instance segmentation with a discriminative loss function. In *Proceedings of the IEEE Conference on Computer Vision and Pattern Recognition*, aug 2017.
- [5] K. Fukunaga and L. Hostetler. The estimation of the gradient of a density function, with applications in pattern recognition. *IEEE Transactions on Information Theory*, 21(1):32–40, jan 1975.
- [6] R. Gala, J. Chapeton, J. Jitesh, C. Bhavsar, and A. Stepanyants. Active learning of neuron morphology for accurate automated tracing of neurites. *Frontiers in Neuroanatomy*, 8:37, may 2014.
- [7] M. Johnson-Roberson, C. Barto, R. Mehta, S. N. Sridhar, K. Rosaen, and R. Vasudevan. Driving in the matrix: can virtual worlds replace human-generated annotations for real world tasks? In *Proceedings of the IEEE International Conference on Robotics and Automation*, pages 746–753. IEEE, may 2017.
- [8] D. P. Kingma and J. Ba. Adam: a method for stochastic optimization. In *Proceedings of the 3rd International Conference for Learning Representations*, dec 2014.
- [9] R. Klokov and V. Lempitsky. Escape from cells: deep kd-networks for the recognition of 3D point cloud models. In *Proceedings of the IEEE International Conference on Computer Vision*, pages 863–872, 2017.
- [10] Z. Nougara, N. Kihal, and J. Meunier. Semi-automated extraction of retinal blood vessel network with bifurcation and crossover points. In *International Symposium on Visual Computing*, pages 340–348. Springer, Cham, dec 2016.
- [11] Open Source Medical Software Corporation. <http://www.vascularmodel.com>, 2018.
- [12] E. Park and A. C. Berg. Learning to decompose for object detection and instance segmentation. *arXiv:1511.06449*, 2015.
- [13] X. Peng, B. Sun, K. Ali, and K. Saenko. Learning deep object detectors from 3D models. In *Proceedings of the IEEE International Conference on Computer Vision*, volume 2015 Inter, pages 1278–1286, dec 2015.
- [14] X. B. Peng, M. Andrychowicz, W. Zaremba, and P. Abbeel. Sim-to-real transfer of robotic control with dynamics randomization. *arXiv:1710.06537*, oct 2017.
- [15] H. Pratt, B. Williams, J. Ku, C. Vas, E. McCann, B. Al-Bander, Y. Zhao, F. Coenen, and Y. Zheng. Automatic detection and distinction of retinal vessel bifurcations and crossings in colour fundus photography. *Journal of Imaging*, 4(2):4, dec 2017.
- [16] C. R. Qi, H. Su, M. Kaichun, and L. J. Guibas. PointNet: deep learning on point sets for 3D classification and segmentation. In *Proceedings of the IEEE Conference on Computer Vision and Pattern Recognition*, pages 77–85. IEEE, jul 2017.
- [17] C. R. Qi, L. Yi, H. Su, and L. J. Guibas. PointNet++: deep hierarchical feature learning on point sets in a metric space. In *Advances in Neural Information Processing Systems*, pages 5099–5108, 2017.
- [18] B. Romera-Paredes and P. H. S. Torr. Recurrent instance segmentation. In *European Conference on Computer Vision*, pages 312–329. Springer, Cham, oct 2016.
- [19] H. Schar, M. Minervini, A. P. French, C. Klukas, D. M. Kramer, X. Liu, I. Luengo, J.-M. Pape, G. Polder, D. Vukadinovic, X. Yin, and S. A. Tsafaris. Leaf segmentation in plant phenotyping: a collation study. *Machine Vision and Applications*, 27(4):585–606, may 2016.
- [20] J. Staal, M. D. Abramoff, M. Niemeijer, M. A. Viergever, and B. Van Ginneken. Ridge-based vessel segmentation in color images of the retina. *IEEE Transactions on Medical Imaging*, 23(4):501–509, apr 2004.
- [21] R. Stewart, M. Andriluka, and A. Y. Ng. End-to-end people detection in crowded scenes. In *Proceedings of the IEEE Conference on Computer Vision and Pattern Recognition*, pages 2325–2333, 2016.
- [22] D. Sui, K. Wang, J. Chae, Y. Zhang, and H. Zhang. A pipeline for neuron reconstruction based on spatial sliding volume filter seeding. *Computational and mathematical methods in medicine*, 2014:386974, jul 2014.
- [23] Y. Taigman, A. Polyak, and L. Wolf. Unsupervised cross-domain image generation. *arXiv:1611.02200*, nov 2016.
- [24] J. Tobin, L. Biewald, R. Duan, M. Andrychowicz, A. Handa, V. Kumar, B. McGrew, J. Schneider, P. Welinder,

- W. Zaremba, and P. Abbeel. Domain randomization and generative models for robotic grasping. In *arXiv:1710.06425*, 2017.
- [25] J. Tobin, R. Fong, A. Ray, J. Schneider, W. Zaremba, and P. Abbeel. Domain randomization for transferring deep neural networks from simulation to the real world. *Proceedings of the IEEE/RSJ International Conference on Intelligent Robots and Systems*, pages 23–30, 2017.
- [26] J. Tremblay, A. Prakash, D. Acuna, M. Brophy, V. Jampani, C. Anil, T. To, E. Cameracci, S. Boochoon, and S. Birchfield. Training deep networks with synthetic data: bridging the reality gap by domain randomization. *arXiv:1804.06516*, 2018.
- [27] E. Tzeng, J. Hoffman, N. Zhang, K. Saenko, and T. Darrell. Deep domain confusion: maximizing for domain invariance. *arXiv:1412.3474*, dec 2014.
- [28] J. Wu, C. Zhang, T. Xue, B. Freeman, and J. Tenenbaum. Learning a probabilistic latent space of object shapes via 3D generative-adversarial modeling. In *Advances in Neural Information Processing Systems*, pages 82–90, 2016.
- [29] Z. Wu, S. Song, A. Khosla, F. Yu, L. Zhang, X. Tang, and J. Xiao. 3D ShapeNets: A Deep Representation for Volumetric Shapes. In *Proceedings of the IEEE Conference on Computer Vision and Pattern Recognition*, pages 1912–1920, 2015.
- [30] J. Yosinski, J. Clune, Y. Bengio, and H. Lipson. How transferable are features in deep neural networks? *Advances in neural information processing systems*, pages 3320–3328, 2014.
- [31] L. Yu, X. Li, C.-W. Fu, D. Cohen-Or, and P.-A. Heng. PU-Net: point cloud upsampling network. In *Proceedings of the IEEE Conference on Computer Vision and Pattern Recognition*, pages 2790–2799, 2018.